ADVANCED ELECTRONIC MATERIALS
www.advelectronicmat.de

Effect of Humidity on the Writing Speed and Domain Wall Dynamics of Ferroelectric Domains

Irena Spasojevic, Albert Verdaguer, Gustau Catalan, and Neus Domingo**

The switching dynamics of ferroelectric polarization under electric fields depends on the availability of screening charges in order to stabilize the switched polarization. In ferroelectrics, thin films with exposed surfaces investigated by piezoresponse force microscopy (PFM), the main source of external screening charges is the atmosphere and the water neck, and therefore relative humidity (RH) plays a major role. Here, it is shown how the dynamic writing of domains in $BaTiO_3$ thin films changes by varying scanning speeds in the range of RH between 2.5% and 60%. The measurements reveal that the critical speed for domain writing, which is defined as the highest speed at which electrical writing of a continuous stripe domain is possible, increases non-monotonically with RH. Additionally, the width of line domains shows a power law dependence on the writing speed, with a growth rate coefficient decreasing with RH. The size of the written domains at a constant speed as well as the creep-factor μ describing the domain wall kinetics follow the behavior of water adsorption represented by the adsorption isotherm, indicating that the screening mechanism dominating the switching dynamics is the thickness and the structure of adsorbed water structure and its associated dielectric constant and ionic mobility.

1. Introduction

The interaction of adsorbed water with ferroelectric (FE) materials such as $BaTiO_3$ has been studied due to its dipolar character and the possibility to split into ionic species (i.e., OH^- and H^+) (dissociation).[1–8] Consequentially, water plays a crucial role in the screening of the depolarization field and the stabilization of FE polarization in the absence of electrodes capable of supplying free charge.[9–12] This screening role is of particular importance in thin films studied by piezoresponse force microscopy (PFM), where the stability of patterned domain arrays (i.e., bits) is ruled by screening processes and is a prerequisite for information storage applications, where long-time data retention is needed.[13] Besides stabilizing polarization, it has been long known that switching dynamics is also affected by adsorbed water and therefore relative humidity (RH),[14–20] since nucleation and growth of domains depend on the distribution of electric fields around the AFM tip and the mobility of ionic screening charges.

So far, however, studies concerning size evolution of written domains with RH are inconsistent. The majority of works demonstrate that the size of written domains at constant bias grows linearly with RH,[17,18,21] but some authors report on nonlinear decrease of domain size at high RH.[16,22] Up to know, switching experiments were conducted for high RH between 20% and 90%, and studies in low RH conditions have not yet been performed. Studies of switching dynamics in the dry range are of particular interest because important processes such as chemisorption of anchoring hydroxyl groups and physisorption of the first water layers are expected to take place, having strong influence on diffusional mobility of ionic compensating species.[23–25]

It is also important to point out that all previous studies of switching dynamics were conducted in a static mode, by applying pulses of different intensities and lengths to a biased AFM tip placed in contact at a fixed point of the substrate.[13,14,16–18,21,26] Seminal works lead by Gruverman[27,28] and Paruch et al.,[13,29] studying the dynamics of ferroelectric domain growth kinetics under tip generated electric fields stablish the exponential dependence of the lateral domain wall velocity with the field and the domain size, which is further modulated by a dynamical exponent μ when domain walls motion is governed by a creep process. However, encoding of ferroelectric bits is a dynamic process, and in some proposed setups bit rate is limited by the successfulness

I. Spasojevic, G. Catalan, N. Domingo
Catalan Institute of Nanoscience and Nanotechnology (ICN2)
CSIC and BIST
Campus UAB
Bellaterra, Barcelona 08193, Spain
E-mail: gustau.catalan@icn2.cat; neus.domingo@icn2.cat

I. Spasojevic
Department of Chemistry
Universitat Autònoma de Barcelona
Bellaterra, Barcelona 08193, Spain

A. Verdaguer
Institut de Ciència de Materials de Barcelona (ICMAB)
CSIC
Campus UAB
Bellaterra, Barcelona 08193, Spain

G. Catalan
ICREA - Institució Catalana de Recerca i Estudis Avançats
Catalonia, Barcelona 08010, Spain

The ORCID identification number(s) for the author(s) of this article can be found under https://doi.org/10.1002/aelm.202100650.

DOI: 10.1002/aelm.202100650

of switching events at the given scanning speed: as the speed of rotation of a "ferroelectric record disk" is increased, successful single bit writing by a PFM tip decreases.[30,31] This behavior might be related to the insufficient population of surface screening charges capable of stabilizing the newly formed domains at sufficient speed. Although kinetics of domain growth can be tuned by RH, studies that concern of the interplay between scanning speed and RH on domain switching are still lacking.

In this work, we explore the influence of RH on the critical speed for the linear domain writing, by driving a biased AFM tip across the ferroelectric $BaTiO_3$ thin film surface using different speeds and in distinct RH conditions. Further on, we study domain size dependence on ferroelectric writing speed and applied tip voltage independently in different RH conditions. All measurements were performed in a wide range of writing speeds and RH, including the low-humidity range all the way down to 2.5% humidity. This enabled us to construct the map of domain size evolution as a function of these parameters and correlate observed behavior with dominant screening mechanisms involved, closely related to water adsorption processes. As we will show, relative humidity has a strong and positive effect on the maximum speed at which ferroelectric domains can be written, but the effect is non-monotonical, reflecting three distinct regimes in the water adsorption isotherm.

2. Results and Discussion

For this study, we used epitaxial 21 nm thick $BaTiO_3$ (BTO) thin film grown on 33 nm thick $SrRuO_3$ (SRO) conductive buffer layer on a (001) oriented $SrTiO_3$ (STO) substrate by pulsed laser deposition (PLD). The preparation procedure can be found elsewhere.[32] The BTO film was atomically flat, fully epitaxial and uniformly *c*-axis oriented with up-polarized as-grown state, as evidenced by piezoresponse force microscopy (PFM).[32] The writing speed experiments were performed using an Asylum MFP3D AFM with a fluid cell integrated to a low-noise continuous flow humidity controller that by combining dry N_2 gas with distilled water allows high precision control of RH at the cell with long term stability.[33] The minimum value of RH achieved after exposure to pure N_2 gas for 60 h was 2.5%. Once the desired RH was achieved, two sets of consecutive writing experiments were performed: first by applying an increasingly positive voltage to the AFM tip at a constant writing speed, and second by setting a constant applied voltage and increasing the writing speed, respectively. All domains were written dynamically in the shape of lines. For each voltage/scanning speed combination, two consecutive lines were written to verify repeatability. In order to achieve stable tip-sample coupling, two extra lines were written at the beginning of each experiment

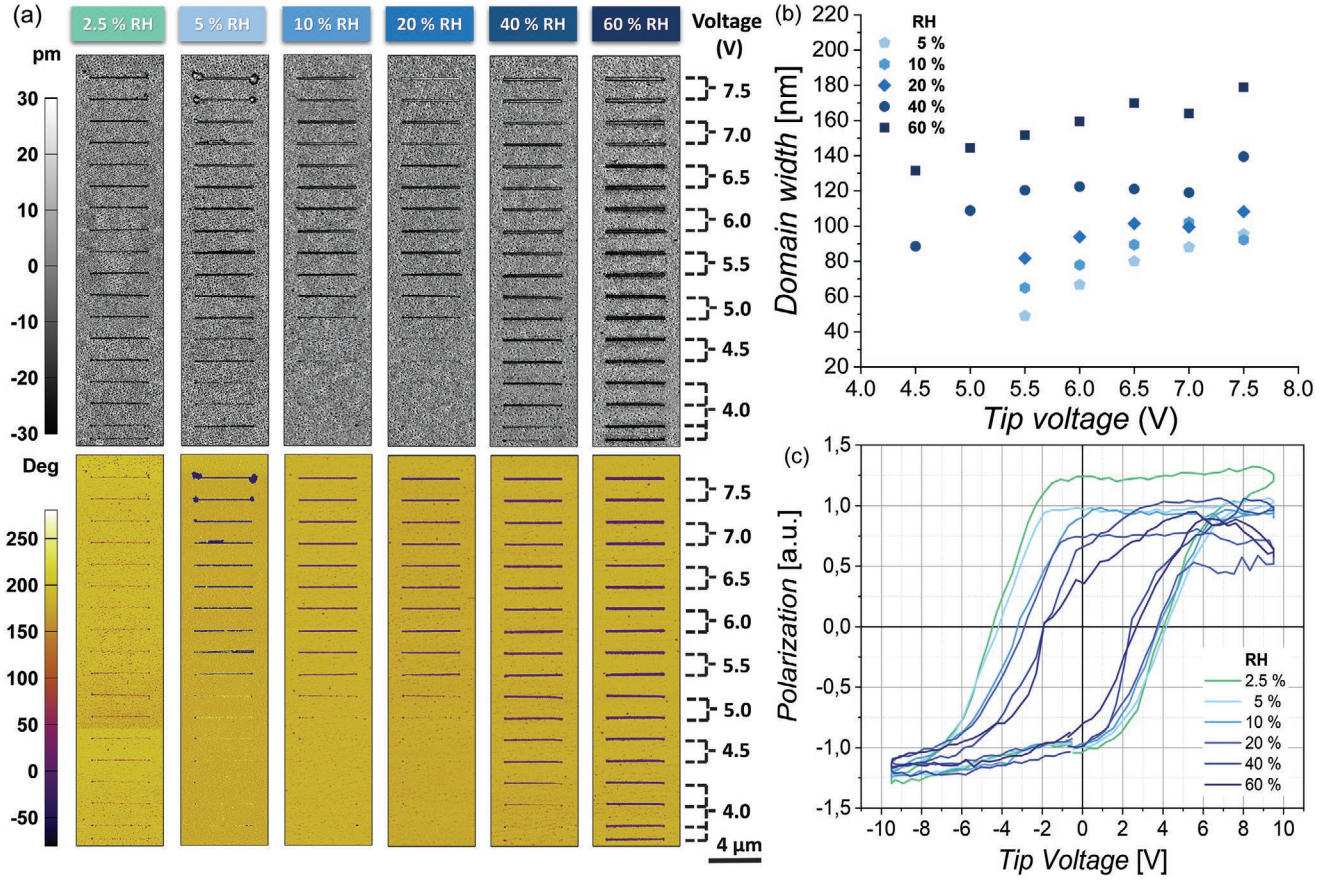

Figure 1. a) PFM amplitude and phase images of down-polarized lines written in different RH conditions by increasing writing voltage, using a Nanosensors EFM tip ($k \approx 2.8$ N m^{-1}, $r = 30$ nm) at the constant speed of 12.47 µm s^{-1} and contact force of 100 nN. b) Domain width evolution as a function of applied tip voltage for the constant speed of 12.47 µm s^{-1} and for different RH. Domain width increases with voltage and RH until reaching a saturation value; c) Hysteresis loops measured by SS-PFM at 0.2 Hz in different RH conditions showing decrement of coercive voltage with RH.

at the lowest speed/voltage conditions. In all the experiments, a Nanosensors EFM tip ($k \approx 2$ N m^{-1}) was used at a constant force of 100 nN. Then, the obtained pattern of written lines was measured by PFM as shown in **Figure 1**a, and the line thicknesses that correspond to domain width were calculated from the average number of pixels in the PFM phase images.

In order to characterize the switching response, we apply "writing" voltages in the range from 4.5 to 7.5 V to the AFM tip while scanning straight lines in contact mode at a constant speed of 12.47 µm s^{-1} and in different RH conditions. When the voltage is sufficiently large, "line domains" appear in the tip's wake, with a width that, like the diameter of point-domains,[18] grows proportionally to the excess voltage above coercivity. This is shown in Figure 1a. Extracting the quantitative information from the maps, we see (Figure 1b) that indeed domain width increases with voltage, until reaching a saturation value. We also observe that the width of the line domains not only depends on applied voltage but also on humidity: for any given voltage, domain width increases with increasing humidity. Moreover, the saturation width is larger, and is reached at lower voltages, as humidity is increased. The results indicate that surface water and related adsorbates facilitate switching and stabilize the switched domains by providing the requisite screening charge. This conclusion is also supported by the switching spectroscopy PFM measurements[34] on up-polarized BTO thin film as a function of RH shown in Figure 1c. It can be seen that coercive field decreases when the RH is raised from 5% to 60% RH. The symmetry of the hysteresis curve is also in agreement with similar studies[20] and the observed imprint is well explained by the influence of surface screening on the domian nucleation[35] and initial growth stages during hysteresis loops.[36]

2.1. Effect of Relative Humidity on the Writing Speed of Ferroelectric Domains

Having established that water facilitates FE switching both in hysteresis loops and in FE lithography, next we explore how humidity affects the FE the writing speed. To address this issue, we perform a new set of FE lithography measurements where, instead of fixing the scanning speed and increasing voltage, we fix the voltage and increase the scanning speed. **Figure 2**a shows

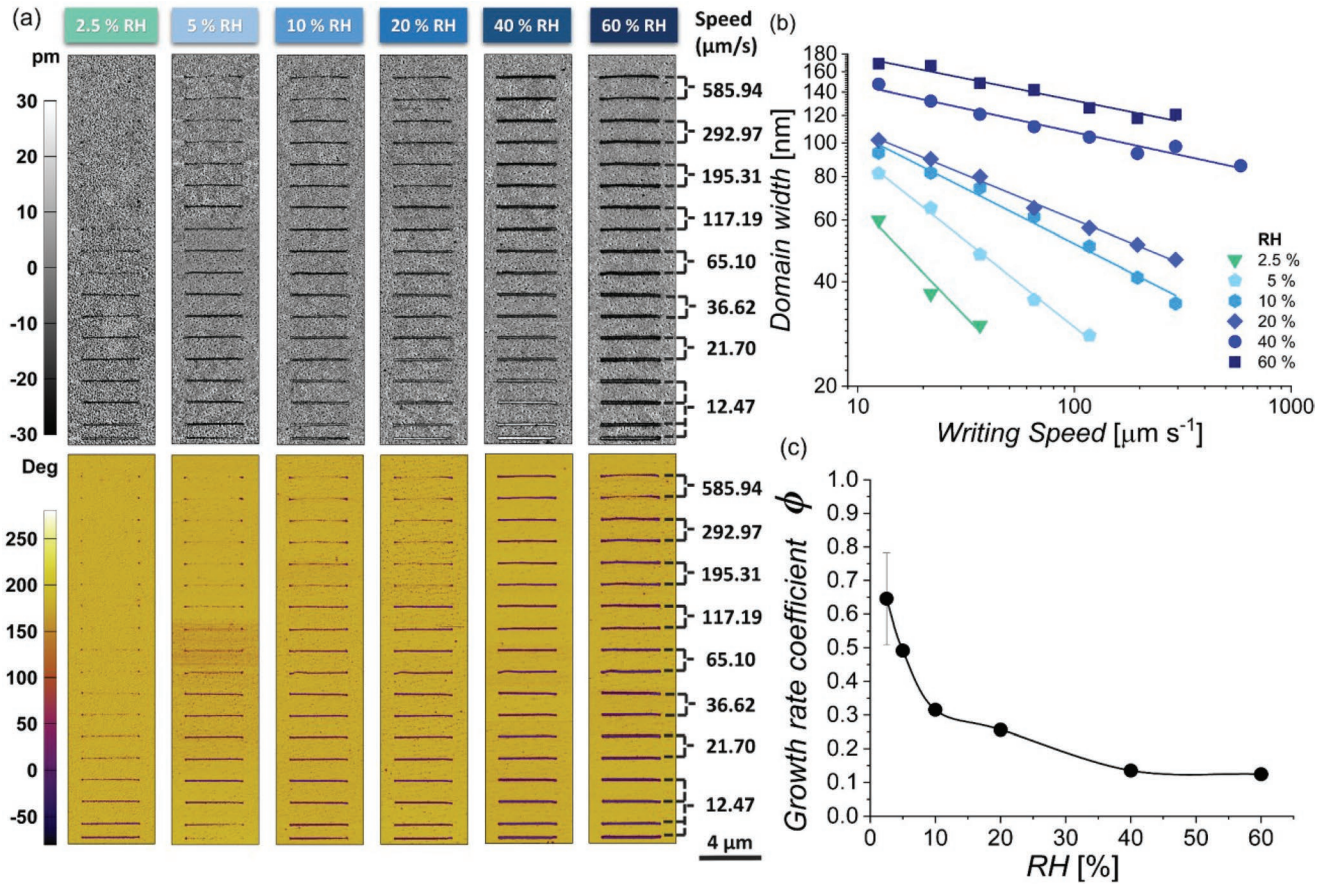

Figure 2. a) PFM amplitude and phase images of down-polarized lines written in different RH conditions by increasing writing speeds and at a constant tip bias of 6.5 V while scanning using a force of 100 nN. Critical writing speed is shifting towards higher values as RH is increased; b) Measured domain width as a function of writing speed for different RH showing a power law dependence (Equation (1)); c) Slopes of the fitted data from Figure 2b with Equation (1) as a function of RH. Absolute values of growth rate coefficient decrease with the rise of RH, achieving a plateau at high RH and revealing that the domain width is more sensitive to the writing speed in the low RH range. Note that the differences in writing at 2.5% RH using the speed of 12.5 µm s^{-1} between Figure 1a and Figure 2a, might stem from the slight changes in experimental parameters, most probably the stability of water meniscus between the tip and the sample caused by discontinous water coverage at low RH or small changes in the coercive voltages. In low RH conditions, slight changes of mentioned parameters can have strong influence on the delicate balance between depolarization fields and scarce external screening charges.

the PFM amplitude and phase images of down-polarized lines written in different RH conditions by using a constant bias of 6.5 V and increasing writing speeds in the range from 12.47 to 585.94 μm s^{-1}. At each RH, the width of the lines decreases and gradually disappears for increasing writing speeds. We define the critical speed of writing as the highest speed for which homogeneous writing (a continuous line domain) is observed for each RH condition. It can be seen that the critical speed shifts towards higher values as RH is increased, and at 40% RH all the lines are written successfully, independently of the used scanning speed within our experimental range. The increase in the critical speed for writing confirms that humidity facilitates switching.

To further study the RH influence in the dynamics of the ferroelectric polarization switching, we need to distinguish two different axis for the dynamics: the direction along the tip displacement, characterized by the tip scanning speed, i.e., the writing speed S, and the transversal axis perpendicular to the writing direction, where the domain growth is determined by a creep regime with a characteristic time depending on the inverse of the tip scanning speed. Previous studies of domain wall kinetics observed that the domain size scales approximately logarithmically with the writing time and in general it is best fitted by a power law $w \approx t^{\phi}$,[37] with the growth rate coefficient ϕ taking values $\phi < 1$.[15,19,38] Correspondingly, in our case time scales with the inverse of the tip scanning speed S ($t \approx 1/S$). We have fitted our experimental that in Figure 2b following Equation (1)

$$\log w = K - \varnothing \cdot \log S \quad (1)$$

where w is the line width, K is a constant, S is the tip velocity and ϕ is the growth rate coefficient. The growth rate coefficient ϕ is observed to decrease as RH increases, i.e., for 2.5% RH $\phi = 0.64$ and decreases to $\phi = 0.26$ for 20% RH, achieving a plateau above 40% RH (Figure 2c). This means that the line width is more sensitive to the writing speed in the low RH range, i.e., under 10%: the high values of the growth rate coefficient for low RH indicate that domain width decreases faster with speed.

Figure 3a shows iso-width lines as a function of RH and writing speed. Every symbol represents a combination of RH and writing speed for which a writing experiment has been performed. Full, half-filled and empty symbols denote conditions for which either complete, partial or unsuccessful writing has been observed, respectively. For our experiment, where we used a tip with a nominal radius of R = 50 nm, the minimal observed widths of dashed and fully written lines are 30 and 48 nm, respectively. The iso-width lines represent combinations of RH and tip velocity for which a given domain width is achieved. These lines were calculated from the fitting parameters of Figure 2b by choosing the desired input values of speed and then calculating predicted values of domain width at each RH. Iso-width lines are obtained by connecting the coordinates (RH, Speed) that give the same value of calculated domain width. The color scale is the whole distribution map of domain width vs writing speed and RH. The white region denotes combinations of RH and tip scanning speed for which scanning is too fast or humidity too low for domains to be written at all, and therefore the edge of the white region represents the critical writing speed for each RH where domains disappear altogether.

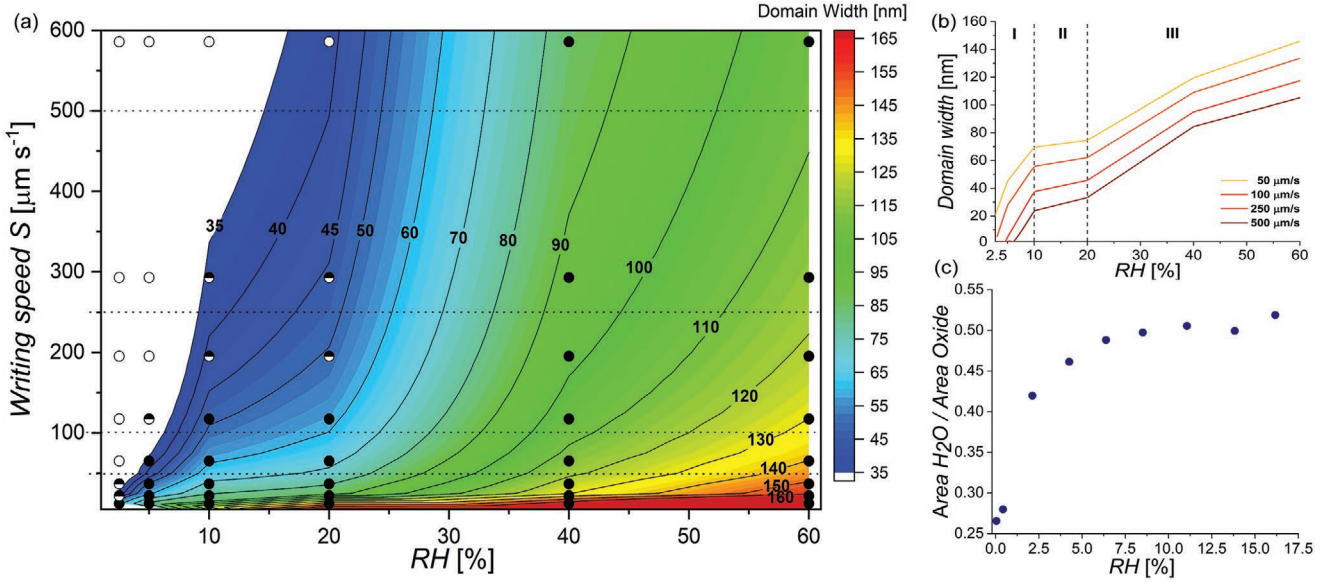

Figure 3. a) Color map showing the domain width dependence on the writing speed and RH. Symbols correspond to experimental points of RH and speed for which writing experiment has been performed with full, half-filled and empty symbols denoting conditions for which complete, partial and unsuccessful writing has been observed. Iso-width lines are obtained by connecting the coordinates (RH, Speed) that give the same value of calculated domain width, predicted by using fitting parameters of Figure 2b; b) Cross sections of domain width map at four arbitrary chosen writing speeds, showing non-monotonic growth of the domain width with RH at the constant writing speed. Shape of the domain width vs RH closely resembles the shape of adsorption isotherm of water on $BaTiO_3$ and similar oxide materials in different RH conditions, which correlates amount of adsorbed water as a function of RH. c) Area of the water peak normalized by the area of bulk oxide peak in O1s spectrum obtained by AP-XPS measurements as a function of RH, representing adsorption isotherm of water on BTO surface in low to intermediate RH range.

Cross sections along the black horizontal lines of the color map in Figure 3a yield the dependence of domain width on RH for arbitrarily chosen writing speeds. A few such lines are plotted in Figure 3b. Several interesting features emerge from this graph. Above 20% humidity, the line width is an almost-linear function of the RH, which is in good agreement with the only reported study so far, where the domain diameter was examined as a function of RH for RH > 30% and different pulse times.[18] However, at low RH the behavior is non-monotonic, showing a plateau of constant domain width between 10% and 20%, and a non-linear dependence at lower humidity that gets increasingly steeper as RH approaches 0.

The physical meaning of the power law relationship between line domain width and writing speed is more intuitive when looked at in reverse: in a creep regime, the time required for a point-contact domain to reach a given diameter is a power law of the diameter. Translated to line-writing, domain diameter becomes line domain width, and the writing time for each point along the line is inversely proportional to writing speed. Hence, writing speed must be slowed down logarithmically in order to hit a given domain width. Conversely, line domain width decreases logarithmically with writing speed (Equation (1)) as shown by the experimental results. This fact can be explained in terms of external screening dynamics: when there is no sufficient external screening charge available for the screening of newly written domains, the insufficient amount of surface adsorbates strongly affects successfulness of line writing.

In static conditions, the size of the written domains depends on the lateral size of the water meniscus formed between tip and sample and on the ability of ionic species (such as H^+, OH^-, and H_3O^+) to adsorb and diffuse on the surface to perform the necessary screening.[16,18] The water meniscus is formed by capillary condensation of water vapor in the small gap between the tip and the sample and typically grows until the thermodynamic equilibrium through surface adsorption and transport of water molecules from the surface (see detailed description in the Supporting Information). The overall time scale for the meniscus formation is of the order of several milliseconds,[39] which is in the limit of the total time spent in our experiments to move the tip one single step of $\Delta x = 100$ nm at the lowest writing speed of 12.5 μm s^{-1}. On the other hand, further increase of water neck volume until saturation is observed to take up to hundreds of seconds,[40,41] which is well above the total time used to write a full line of 4 μm, which takes 320 ms at the lowest speed. This fact rules out the influence of water meniscus on the growth rate and size of our ferroelectric domains since in almost all our experiments in dynamic conditions, even the water neck is formed, it doesn't have time to grow to saturation. Moreover, low influence of the water meniscus is also expected in the electric field distribution around the AFM tip, as shown by previous simulations.[18]

Still, the water meniscus is a clear source of ionic charges such as protons and hydroxil groups among others, since a portion of water molecules will dissociate under the application of high voltages, thus becoming the closer sink of screening agents. However, the efficiency on surface polarization screening by ions generated or concentrated at the water neck, similarly to Dip Pen nanolithography, will strongly depend on the transport rates of charges through the neck and more specifically their diffusion rate at the surface. The obtained relationship of the domain size as a power law of the writing speed points to fact that the diffusion of ionic charges at the surface is indeed the dominant factor in surface screening.[42,43]. In this case, the diffusion of ionic charges depends on surface conductivity which will be essentially dominated not only by the amount of water adsorbed on the surface but also on its structure.

The process of water adsorption is governed by RH conditions via the adsorption isotherm,[44] which relates the thickness of the adsorbed water layer to the relative pressure or RH at constant temperature. Nonetheless, the contribution of water structure, dictated by water adsorption and RH, on ferroelectric domain screening has not been considered up to now. In order to delve into the adsorption of water on our $BaTiO_3$ thin film surfaces, we measured a set of oxygen O 1s spectra in distinct RH conditions by the means of Ambient Pressure X-Ray Photoelectron Spectroscopy (AP-XPS). With this technique, XPS measurements were conducted in the range of RH between 0% and maximum of ≈17% (low and intermediate RH ranges) by increasing the water vapor pressure of the XPS chamber from UHV to 4 mbar. Obtained O 1s spectra were fitted following the model explained in detail in our previous works,[6,32] which enabled us to quantify the amount of molecular water adsorbed at every RH. The area of the molecular water peak normalized by the area of bulk oxide peak, which gives the information about the amount of water isothermally adsorbed on the surface, has been plotted as a function of RH and shown in Figure 3c. It can be seen that at low RH up to ≈ 10%, water adsorbs on BTO surface in non-linear fashion, reaching a plateau of constant water content between 10% and ≈17% of RH. The shape of the adsorption isotherm of water on our BTO surfaces in the measured RH range (Figure 3c), is in good agreement with the trend observed on similar different oxide surfaces[24,45–47] (note that in any case, the final calculation of water thickness in monolayers depends on the structure of the adsorbates layer and also the evolution of the other available species with RH, which can lead to a more pronounced slope for low RH) and is remarkably similar to the shape of the domain width vs RH depicted in Figure 3b, suggesting a link between the two. Each of these curves consists of three regions corresponding to different range of RH: a first region of steep increase in adsorbate thickness/domain width as a function of humidity, a second region with a plateau, and a third region where adsorbates layer thickness and domain size grow again. This trend is depicted as well in the growth rate coefficient as a function of RH.

The low-humidity range in our FE dynamic lithography experiments comprises RH between 2.5% and 10% RH. Previous studies established that hydroxyl (OH) groups available from water-splitting reactions[2,3,6] get strongly chemisorbed onto the surface immediately after exposing the sample to the ambient conditions from the vacuum preparation chamber. Therefore, our starting point is an already hydroxylated surface, even in the lowest RH conditions with a sub-monolayer water layer below RH ≈ 10%,[48] indicating that in this regime the surface water coverage is discontinuous at best. Water molecules in the sub-monolayer up to the first monolayer state are tightly bound to the surface (Figure 3b, Region I), leading to the formation of a highly structured water layer with very low dielectric constant[24,49,50] which could reach values around $\varepsilon \approx 2$, and where rotation or diffusion of water molecules is

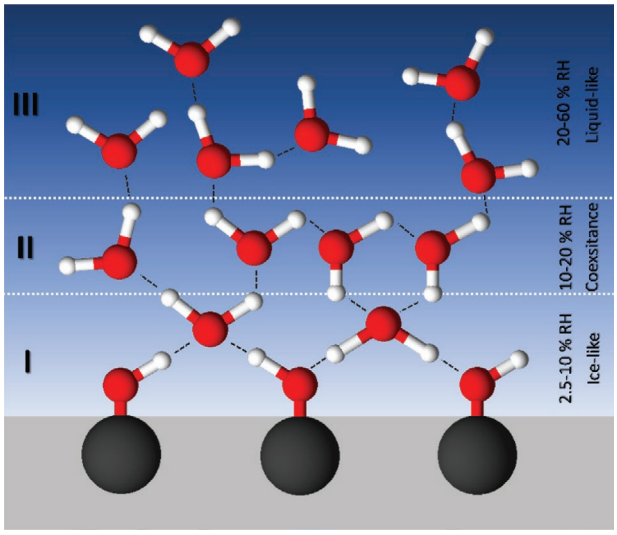

Figure 4. Schematic representation of the water structures expected on BTO surface as a function of increasing RH. I) Highly structured ice-like water layer where hydrogen bonds are formed between chemisorbed OH groups and upcoming water molecules (represented by dashed lines). This immobilized ice-like water layer is characterized by low dielectric constant of water molecules and hindered mobility of water and ionic species; II) Coexistence between highly structured and liquid-like water growth structures with a higher dielectric constant and therefore higher capacity for dipolar screening but still limited ionic mobility; III. Stabilization of liquid-like water layers with maximized ionic mobility.

very limited.[51] Therefore, in this highly structured water layer dipolar screening by water molecules reorientation is negligible. On the other hand, mobility of ionic charges mediated by hoping of H^+ and OH^- through the chain of water molecules bound by H-bonds is also strongly affected by water structure and therefore RH.[52] Ab initio molecular simulations confirmed that proton transfer rate substantially decreases going from a liquid-like multilayer to the rigid monolayer coverage on a ZnO surface, following the associated change on the water structure.[53] In **Figure 4** are schematicaly represented different water structures that can be expected on BTO surface as a function of increasing RH.

In this regime, polarization screening mechanisms assisting FE polarization switching and stabilization, mediated by the change of the chemisorbed layer and/or redistribution of ionic charges in the area of newly formed domain, will be highly innefficient due to the limited water dipoles and ionic mobility in this low RH range. Moreover, existence of incomplete monolayer of water could additionally affect the already limited mobility of ionic charges over longer ranges. The experimental evidence indicates that, at sufficiently fast scanning speeds, neither of these processes is fast enough to keep up with the screening demands of a switched polarization, and probably writing efficiency is limited by domain nucleation and internal screening mechanisms. As humidity goes up, the increased mobility of ionic species in liquid-like water layers favors a faster screening-charge dynamics.[23,52]

The region between 10% and 20% RH is characterized by stagnation of the initial growth of domain width vs RH (Figure 3b, region II). After the first monolayer of water is formed, subsequent water layers feel weaker influence from the hydroxylated substrate and adsorb in a less ordered manner, such that some water molecules are becoming mobile on the surface and have a structure similar to the bulk liquid water. Therefore, the plateau between 10% and 20% RH represents coexistence between two water-growth structures, schematicaly represented in the Figure 4, with different kinetic behavior: 1) highly ordered, surface immobilized water and 2) mobile, liquid-like water molecules. Moreover, the barrier for protonic mobility by hoping is decreasing with increasing RH, giving the overall rise of the protonic conductivity of thicker water layers.[53,54] Therefore, higher protonic conductivity together with increased mobility and orientational freedom of water molecules in this region might play crucial role in the polarization screening, finally enabling successful writing of ferroelectric domains even when high speeds are used.

At higher RH, i.e., above 20%, water forms a highly mobile liquid structure that characterizes region III in Figure 3b. Previous studies of domain size for different pulse duration and RH show similar monotonic increase in the range of RH from 28% to 65%.[18] The most natural explanation for this behavior is that, once a continuous layer of liquid-like water has condensed on the entire surface of the ferroelectric film, ions can easily migrate to assist the screening process. The approximately linear relationship between domain size and RH for any given scanning speed (range III in Figure 3b) (or, equivalently, for any given switching time[18]) would be a direct evidence of the increasing thickness of the transport layer (the liquid), since conductivity (ionic, in this case) is linearly proportional to the thickness of the conductor. Therefore, for RH above 10% we can consider that the dominating screening mechanisms are driven by the progressively increase of surface adsorbate layer such as water and associated improve of the conductivity and difussion of its dissociation products such as H^+, OH^-, and H_3O^+ ions.

2.2. Effect of the Relative Humidity on the Transversal Domain Wall Dynamics

If we now consider the dynamics in the transversal axis, we can calculate the domain growth rate of the domains perpendicular to the writing direction. To do so, we multiply the domain width by the tip scanning speed to obtain an average growth velocity $v = w \cdot S$, describing the domain wall dynamics per unit of linear nanometer as a function of RH. The domain growth velocity in creep regimes depends on the domain wall motion, which has been traditionally described as governed by wall pinning in defect sites.[18,55] The motion of domain walls governed by creep processes is described by the velocity of observed lateral domain expansion taking the form

$$v = v_\infty \exp\left[-\frac{U_a}{kT}\left(\frac{E_c}{E}\right)^\mu\right] \quad (2)$$

where μ is the dynamical exponent, U_a is the characteristic activation energy, $E_c >> E$ is the critical electric field, T is the temperature and k is the Boltzmann's constant. If we consider that $E \approx 1/w$, then Equation (2) can be simplified and we obtain the following logarithmic relationship for the domain growth velocity v and the final domain size w[56]

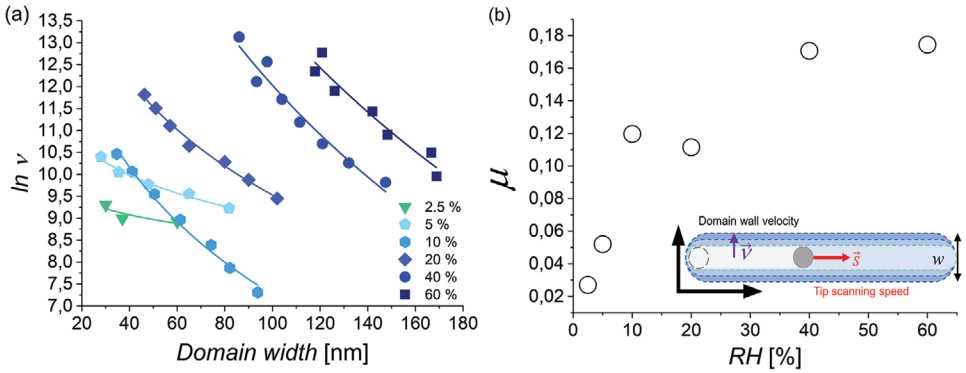

Figure 5. a) Exponential dependence of the domain growth velocity along the transversal axial direction on the domain width for different relative humidities. The continuous lines correspond to the fitting of the data with Equation (3), using the dynamic coefficient μ plotted in (b) for the different curves. The fittings share the same K values for all RH. The inset shows the scheme of the two axes where dynamics have been studied.

$$\ln v = \ln v_{\infty} - K \cdot w^{\mu} \tag{3}$$

In this framework, deviations of the dynamical exponent from $\mu = 1$, corresponding the the domain wall motion in a defect-free crystal lattice, have been explained by a creep-like motion of the domain boundary. **Figure 5**a shows the fitting of Equation (3) to the experimental data, with the dynamical exponents plotted in Figure 5b as a function of the RH. In this case, a stiff increase of the dynamical exponent with increasing RH from 0% to 10% is observed, followed by an abrupt change between 10% and 20% of RH, until a plateau is finally reached for RH ≥ 40%.

The enhanced mobility of the screening charges as a function of RH as discussed in the previous section seems to have a clear impact on the dynamical exponent μ describing the creep motion of ferroelectric domain walls and domains as observed in Figure 5b. Traditionally, the divergence of the growth rate of domains from a linear behavior given by μ =1 in Equations (2) and (3) has been explained in terms of domain wall pinning in bulk defects during growth. For uniform electric fields, the observed domain dynamics have been determined as a balance between the rate of screening charge accumulation and domain boundary velocity.[57] The observed strong dependence of the dynamical exponent with RH, especially for RH < 10% suggests that albeit the density of defects and pinning sites can be influenced by the presence of surface water, there is a direct impact of surface conductivity on the domain wall kinetics probably mediated by the dependence of the electrostatic boundary conditions on the amount of surface water. In this sense, a more general domain wall friction model including the impact of surface water structure on surface ionic conductivity is needed.[58]

3. Conclusions

To summarize, we find that the critical speed for domain writing is highly dependent on RH. While for RH above 20% domains can be written at speeds of 0.6 mm s^{-1} or faster, in dry atmospheres with RH below 5% the critical writing speed slows down to below 100 μm s^{-1}. The size of written line domains depends logarithmically on the writing speed, showing higher growth rate coefficient ϕ, and therefore higher sensitivity of domain size to the writing speed, for the lowest measured RH, caused by the restricted dipolar screening and/or low mobility of ionic species in this low RH conditions.

For a given writing speed (i.e., electric field dwell time in dynamic conditions), we identify three distinct dynamic regimes as a function of RH: i) a low humidity regime below 10% RH, characterized by a non-linear growth of the domain width as a function of RH; ii) a transition regime between 10% and 20%, where domain width and growth coefficients as a function of RH meets a plateau; and iii) a high humidity regime above 20% RH with an almost linear growth in domain width vs RH. Quantification of AP-XPS measurements performed on BTO surfaces in controlled RH conditions enabled us to construct the adsorption isotherm for water in the low to intermediate RH ranges. Noting that the size of the written domains as a function of RH and at fixed speed follows the characteristic behavior of water adsorption in different RH conditions, represented by the adsorption isotherm on BTO and other oxides,[24,45–47] we propose that these regimes are consistent with the initial presence of: ice-like highly structured water molecules in regime I, which besides providing low level of dipolar screening also prevent redistribution of surface charges by hopping, necessary in attending the screening demands (and therefore screening becomes slow in a nominally insulating ferroelectric film); ice-like and incomplete liquid-like water coexisting in regime II, with a higher dielectric constant and therefore higher capacity for dipolar screening but still limited ionic mobility, and a complete layer of liquid water on the surface of the film in regime III, which provides efficient screening via fast ionic mobility along the surface.

These findings have further impact on the study of domain wall dynamics. Our measurements demonstrate that the ferroelectric switching and the domain wall motion are governed by two different mechanisms below and above a RH ≈ 10%, even out of thermodynamical equilibrium with environmental water. For RH<10%, the dominant screening might be provided by internal mechanisms due to the low surface conductivity of charges, with a creep-like lateral motion of domain walls pinned by internal defects. For RH>10%, external screening by surface charges becomes more efficient for the stabilization of ferroelectric switched domains, and ferroelectric switching dynamics depend on the surface charge conductivity, which is modulated not only by the presence of water but also by its

structure when isothermally adsorbed on a surface, leading to increased levels of conductivity with water thickness. In this regime, the dynamics of the domain wall motion should be revisited to account for the water induced change in the electrostatic boundary conditions as a function of its structure.

The present results indicate that, if PFM-based schemes for writing ferroelectric memories are to be implemented,[30] their performance limits in dry-atmosphere conditions will have to be taken into account; otherwise, a ferroelectric memory record that works well in Dublin may not work so well in Dubai. Conversely, the results also highlight how PFM studies of ferroelectric switching open another window into the complex physics of water adsorption and hydrolysis.

Supporting Information

Supporting Information is available from the Wiley Online Library or from the author.

Acknowledgements

The authors want to acknowledge technical support from I. Gaponenko on the installation of the low-noise humidity controller. Financial support was obtained under projects from the Spanish Ministerio de Ciencia e Innovacion (MICINN) under projects PID2019-108573GB-C21, PID2019-109931GB-I00, and PID2019-110907GB-I00. In addition, this work was partially funded by 2017-SGR-579 from the Generalitat de Catalunya. The ICN2 was funded by the CERCA programme / Generalitat de Catalunya. The ICN2 was supported by the Severo Ochoa Centres of Excellence Programme, funded by the Spanish Research Agency (AEI, Grant no. SEV-2017-0706). The ICMAB was supported by the "Severo Ochoa" Program for Centers of Excellence in R&D (CEX2019-000917-S). I.S. acknowledges support of the Secretaria d'Universitats i Recerca - Departament d'Empresa i Coneixement - Generalitat de Catalunya and the European Social Fund (ESF) (FI grant reference 2020 FI_B2 00157). [Correction added on 21 June 2022, after first online publication: figure 2 was replaced.]

Conflict of Interest

The authors declare no conflict of interest.

Data Availability Statement

The data that support the findings of this study are available from the corresponding author upon reasonable request.

Keywords

$BaTiO_3$ thin films, domain wall velocity, ferroelectric polarization switching, relative humidity, screening, water adsorption, writing speed

Received: June 25, 2021
Revised: August 9, 2021
Published online: September 15, 2021

[1] J. L. Wang, B. Vilquin, N. Barrett, *Appl. Phys. Lett.* **2012**, *101*, 092902.
[2] J. L. Wang, F. Gaillard, A. Pancotti, B. Gautier, G. Niu, B. Vilquin, V. Pillard, G. L. M. P. Rodrigues, N. Barrett, *J. Phys. Chem. C* **2012**, *116*, 21802.
[3] X. Li, B. Wang, T. Y. Zhang, Y. Su, *J. Phys. Chem. C* **2014**, *118*, 15910.
[4] H. Lee, T. H. Kim, J. J. Patzner, H. Lu, J. W. Lee, H. Zhou, W. Chang, M. K. Mahanthappa, E. Y. Tsymbal, A. Gruverman, C. B. Eom, *Nano Lett.* **2016**, *16*, 2400.
[5] K. Suzuki, T. Hosokura, T. Okamoto, J. Steffes, K. Murayama, N. Tanaka, B. D. Huey, *J. Am. Ceram. Soc.* **2018**, *101*, 4677.
[6] N. Domingo, E. Pach, K. Cordero-Edwards, V. Pérez-Dieste, C. Escudero, A. Verdaguer, *Phys. Chem. Chem. Phys.* **2019**, *21*, 4920.
[7] G. Geneste, B. Dkhil, *Phys. Rev. B: Condens. Matter Mater. Phys.* **2009**, *79*, 235420.
[8] N. Tymińska, G. Wu, M. Dupuis, *J. Phys. Chem. C* **2017**, *121*, 8378.
[9] S. V. Kalinin, D. A. Bonnell, *Phys. Rev. B: Condens. Matter Mater. Phys.* **2001**, *63*, 125411.
[10] D. Y. He, L. J. Qiao, A. A. Volinsky, *J. Appl. Phys.* **2011**, *110*, 074104.
[11] S. Hong, S. M. Nakhmanson, D. D. Fong, *Rep. Prog. Phys.* **2016**, *79*, 076501.
[12] H. Lu, A. Lipatov, S. Ryu, D. J. Kim, H. Lee, M. Y. Zhuravlev, C. B. Eom, E. Y. Tsymbal, A. Sinitskii, A. Gruverman, *Nat. Commun.* **2014**, *5*, 5518.
[13] P. Paruch, T. Tybell, J. M. Triscone, *Appl. Phys. Lett.* **2001**, *79*, 530.
[14] D. Dahan, M. Molotskii, G. Rosenman, Y. Rosenwaks, *Appl. Phys. Lett.* **2006**, *89*, 152902.
[15] V. Y. Shur, A. V. Ievlev, E. V. Nikolaeva, E. I. Shishkin, M. M. Neradovskiy, *J. Appl. Phys.* **2011**, *110*, 052017.
[16] A. V. Ievlev, A. N. Morozovska, V. Y. Shur, S. V. Kalinin, A. V. Ievlev, A. N. Morozovska, V. Y. Shur, S. V. Kalinin, *Appl. Phys. Lett.* **2014**, *104*, 092908.
[17] K. W. Park, H. Seo, J. Kim, D. Seol, J. Hong, Y. Kim, *Nanotechnology* **2014**, *25*, 355703.
[18] C. Blaser, P. Paruch, *New J. Phys.* **2015**, *17*, 013002.
[19] E. V. Shishkina, E. V. Pelegova, M. S. Kosobokov, A. R. Akhmatkhanov, P. V. Yudin, A. Dejneka, V. Y. Shur, *ACS Appl. Electron. Mater.* **2021**, *3*, 260.
[20] H. Wang, K. Zeng, *Materials* **2021**, *14*, 2447.
[21] S. M. Neumayer, E. Strelcov, M. Manzo, K. Gallo, I. I. Kravchenko, A. L. Kholkin, S. V. Kalinin, B. J. Rodriguez, *J. Appl. Phys.* **2015**, *118*, 244103.
[22] A. V. Ievlev, S. Jesse, A. N. Morozovska, E. Strelcov, E. A. Eliseev, Y. V. Pershin, A. Kumar, V. Y. Shur, S. V. Kalinin, *Nat. Phys.* **2013**, *10*, 59.
[23] K. Cordero-Edwards, L. Rodríguez, A. Calò, M. J. Esplandiu, V. Pérez-Dieste, C. Escudero, N. Domingo, A. Verdaguer, *J. Phys. Chem. C* **2016**, *120*, 24048.
[24] D. B. Asay, S. H. Kim, *J. Phys. Chem. B* **2005**, *109*, 16760.
[25] A. Verdaguer, G. M. Sacha, M. Luna, D. F. Ogletree, M. Salmeron, *J. Chem. Phys.* **2005**, *123*, 124703.
[26] J. Y. Son, G. Lee, Y. H. Shin, *Appl. Phys. Lett.* **2009**, *94*, 162902.
[27] B. J. Rodriguez, R. J. Nemanich, A. Kingon, A. Gruverman, S. V. Kalinin, K. Terabe, X. Y. Liu, K. Kitamura, *Appl. Phys. Lett.* **2005**, *86*, 012906.
[28] A. Agronin, M. Molotskii, Y. Rosenwaks, G. Rosenman, B. J. Rodriguez, A. I. Kingon, A. Gruverman, *J. Appl. Phys.* **2006**, *99*, 104102.
[29] P. Paruch, T. Giamarchi, T. Tybell, J.-M. Triscone, *J. Appl. Phys.* **2006**, *100*, 051608.
[30] T. Aoki, Y. Hiranaga, Y. Cho, *J. Appl. Phys.* **2016**, *119*, 184101.
[31] Y. Hiranaga, T. Uda, Y. Kurihashi, H. Tochishita, M. Kadota, Y. Cho, *Jpn. J. Appl. Phys.* **2009**, *48*, 09KA18.
[32] I. Spasojevic, G. Sauthier, J. M. Caicedo, A. Verdaguer, N. Domingo, *Appl. Surf. Sci.* **2021**, *565*, 150288.
[33] I. Gaponenko, L. Gamperle, K. Herberg, S. C. Muller, P. Paruch, *Rev. Sci. Instrum.* **2016**, *87*, 063709.

[34] S. Jesse, A. P. Baddorf, S. V. Kalinin, S. Jesse, A. P. Baddorf, S. V. Kalinin, **2006**, *88*, 062908.
[35] A. K. Tagantsev, G. Gerra, *J. Appl. Phys.* **2006**, *100*, 051607.
[36] A. N. Morozovska, S. V. Svechnikov, E. A. Eliseev, S. Jesse, B. J. Rodriguez, S. V. Kalinin, *J. Appl. Phys.* **2007**, *102*, 114108.
[37] A. Brugère, S. Gidon, B. Gautier, *J. Appl. Phys.* **2011**, *110*, 052016.
[38] A. P. Turygin, M. M. Neradovskiy, N. A. Naumova, D. V. Zayats, I. Coondoo, A. L. Kholkin, V. Y. Shur, *J. Appl. Phys.* **2015**, *118*, 072002.
[39] L. Sirghi, *Langmuir* **2012**, *28*, 2558.
[40] B. L. Weeks, M. W. Vaughn, J. J. DeYoreo, *Langmuir* **2005**, *21*, 8096.
[41] B. L. Weeks, J. J. DeYoreo, *J. Phys. Chem. B* **2006**, *110*, 10231.
[42] A. Urtizberea, M. Hirtz, *Nanoscale* **2015**, *7*, 15618.
[43] K. A. Brown, D. J. Eichelsdoerfer, X. Liao, S. He, C. A. Mirkin, *Front. Phys.* **2014**, *9*, 385.
[44] J. U. Keller, R. Staudt, *Gas Adsorption Equilibria: Experimental Methods and Adsorptive Isotherms*, Springer, Cham, Switzerland **2005**.
[45] X. Deng, T. Herranz, C. Weis, H. Bluhm, M. Salmeron, *J. Phys. Chem. C* **2008**, *112*, 9668.
[46] L. Chen, X. He, H. Liu, L. Qian, S. H. Kim, *J. Phys. Chem. C* **2018**, *122*, 11385.
[47] T. Rakitskaya, A. Truba, G. Dzhyga, A. Nagaevs'ka, V. Volkova, *Colloids and Interfaces* **2018**, *2*, 61.
[48] N. Domingo, I. Gaponenko, K. Cordero-Edwards, N. Stucki, V. Pérez-Dieste, C. Escudero, E. Pach, A. Verdaguer, P. Paruch, *Nanoscale* **2019**, *11*, 17920.
[49] L. Fumagalli, A. Esfandiar, R. Fabregas, S. Hu, P. Ares, A. Janardanan, Q. Yang, B. Radha, T. Taniguchi, K. Watanabe, G. Gomila, K. S. Novoselov, A. K. Geim, *Science.* **2018**, *360*, 1339.
[50] A. Calò, N. Domingo, S. Santos, A. Verdaguer, *J. Phys. Chem. C* **2015**, *119*, 8258.
[51] B. P. Dhonge, S. S. Ray, B. Mwakikunga, *RSC Adv.* **2017**, *7*, 21703.
[52] A. Verdaguer, J. J. Segura, J. Fraxedas, H. Bluhm, M. Salmeron, *J. Phys. Chem. C* **2008**, *112*, 16898.
[53] G. Tocci, A. Michaelides, *J. Phys. Chem. Lett.* **2014**, *5*, 474.
[54] S. Ø. Stub, E. Vøllestad, T. Norby, *J. Phys. Chem. C* **2017**, *121*, 12817.
[55] P. Paruch, J. Guyonnet, *C. R. Phys.* **2013**, *14*, 667.
[56] N. A. Pertsev, D. A. Kiselev, I. K. Bdikin, M. Kosec, A. L. Kholkin, *J. Appl. Phys.* **2011**, *110*, 052001.
[57] P. Sharma, R. G. P. McQuaid, L. J. McGilly, J. M. Gregg, A. Gruverman, *Adv. Mater.* **2013**, *25*, 1323.
[58] P. V. Yudin, M. Y. Hrebtov, A. Dejneka, L. J. McGilly, *Phys. Rev. Appl.* **2020**, *13*, 14006.